Int. J. Electrochem. Sci., 14 **(2019)** 10396 – 10409, doi: 10.20964/2019.08.158

International Journal of
ELECTROCHEMICAL
SCIENCE
www.electrochemsci.org

Effect of α-tocopherol as a green inhibitor on chloride-induced corrosion of steel

Regina Fuchs–Godec[1,*], *Milorad V. Tomić*[2], *Miomir G. Pavlović*[2]

[1] Faculty of Chemistry and Chemical Engineering, University of Maribor, Smetanova 17, Slovenia,
[2] University of Eastern Sarajevo, Faculty of Technology Zvornik, Karakaj b.b., Republic of Srpska
[*]E-mail: regina.fuchs@um.si

Received: 23 April 2019 / *Accepted:* 25 June 2019 / *Published:* 7 October 2019

Immersion of stainless-steel (SS) samples of type X4Cr13 in ethanol solutions of stearic acid, with and without addition of α-tocopherol, resulted in a modified surface with hydrophobic and corrosion resistance characteristics. We observed a double effect: a hydrophobic and corrosion-resistant surface of SS type X4Cr13 in a solution of 3.0% (wt.) NaCl at 25ºC.
The corrosion properties of bare and modified surfaces of stainless steel were tested by polarization and electrochemical impedance spectroscopy (EIS) in 3.0% (wt.) NaCl solution at 25°C. To observe the morphology and microstructures of sample surfaces, a Scanning Electron Microscope (SEM) was used after the electrochemical measurements. The results obtained from potentiodynamic polarisation measurements show that the inhibition effectiveness of X4Cr13 reached ≈ 68% in cases when surfaces were modified in stearic acid alone (EIS measurements ≈ 82%), while the values increased to more than 99.0% (for both methods) with addition of α-tocopherol (E307). Modification of the surface using an immersion method in an ethanol solution of stearic acid, especially with addition of α-tocopherol, appears to be a promising treatment for improving the corrosion resistance of stainless steel (SS) X4Cr13.

Keywords: green inhibitor, steel, high-level-hydrophobic layer, fat soluble vitamin, aggressive media

1. INTRODUCTION

Corrosion is the process of decay of a material caused by a chemical reaction with its environment. Corrosion of metal occurs when an exposed surface comes in contact with a gas or liquid, and the process is accelerated by exposure to warm temperature, acids, and salts [1-3].

Corrosion has an impact everywhere; it concerns oil companies that pump hot crude through pipelines, military ships and aircraft that spend their active lives at sea, civil engineers designing rebar support for concrete bridges, the automobile industry looking at the effects of road salts or galvanic

couples, and bio-material scientists developing medical splints and joint replacements [4-7]. Corrosion causes disastrous damage to metal and alloy structures causing economic consequences in terms of repair, replacement, product losses, safety and environmental pollution. Among the methods applied to control corrosion, corrosion inhibitors are the most common and economical [8-10], but the most effective inhibitors are toxic and non-biodegradable, thus causing pollution problems [11-14]. Some research groups, however, have reported the successful use of naturally occurring substances to inhibit the corrosion of metals in acidic and alkaline environments [15-27].

Vitamins B and their derivatives have been shown to possess a high inhibitory efficiency against the corrosion of metals in aggressive media [28-31]. Aloysius [28] et al. studied the corrosion inhibition of thiamine hydrochloride (vitamin B1) or biotin (vitamin B7) on mild steel in chloride ion solutions. The adsorption behaviour of vitamin B1 as a corrosion inhibitor for AIS 4130 steel alloy in HCl solutions was studied by Hoseinzadeh et al. [29]. Ramazan Solmaz investigated the corrosion inhibition mechanism and stability of Vitamin B1 on mild steel in 0.5 M HCl solution [30]. The inhibition mechanism and synergistic effect of Lysozyme and vitamin B1 to diversify the application of an inhibitor in an acidic medium were reported by Qiao and co-workers [31].

In this study, we investigate the use of alfa tocopherol (E307- vitamin E) as a corrosion inhibitor on stainless steel in chloride ion solutions. This treatment involves altering some functional surface properties, such as hydrophobicity, in combination with previously mentioned methods. Super-hydrophobic surfaces possess both self-cleaning and low adhesion properties. These surfaces have many practical applications, including separation of oil/water dispersions, drag reduction, anti-bacterial effects, and corrosion and stain resistance. The hydrophobic properties of metal and alloy materials with high surface energies have attracted the attention of researchers because of their widespread use in various industrial and biological applications. Research on super-hydrophobic surfaces has intensified in recent years, and super-hydrophobic films have been successfully fabricated on various metallic substrates, such as stainless steel, copper, bronze, zinc, and aluminium [32-46]. The development of methods to prepare super-hydrophobic surfaces using simple, fast and economic processes is highly desirable. The solution immersion method is a time-saving procedure and needs only cheap reagents. This method is fairly easy to use and no special techniques or equipment are required. A simple chemical method for the fabrication of a super-hydrophobic surface on stainless steel (SS) X4Cr13 was tested for this study. A fat–soluble α-tocopherol (E307- E-vitamin) was used as a type of green inhibitor. After chemical etching in 10% (wt.) HNO_3, the specimens were immediately immersed in a non-stirred, aerated ethanol solution of stearic acid (CH_3 $(CH_2)_{16}COOH$) at room temperature with and without addition of E307. This study is partly an extension of our previous work in which a different corrosion system was used (pure copper was the test material and the corrosion medium was simulated urban rain) [46].

We demonstrate the effectiveness of prepared hydrophobic layers on SS type X4Cr13 within 3.0% (wt.) NaCl at 25°C. Two different electrochemical methods, classical potentiodynamic measurement and electrochemical impedance spectroscopy (EIS), were used for this purpose. A scanning electron microscope (SEM) was used to examine the surface morphology of the self-assembled layers, and a commercial goniometer for testing the wettability of SS type X4Cr13 surfaces

with and without self-assembled layers. Infrared (ATR-FTIR) spectroscopy was used to gain insight into the possible corrosion inhibition mechanism.

2. EXPERIMENTAL

2.1. Materials

Stearic acid (SA) (Sigma–Aldrich, CAS Number 57-11-4) of pure quality (95%) was used without further purification. (+)-α-Tocopherol (E307), a Sigma–Aldrich product, (CAS Number 59-02-9) of pure quality (97%) was also used without further purification. These substances have the following structures (Fig.1):

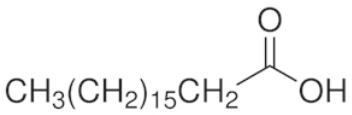

Stearic acid (SA)

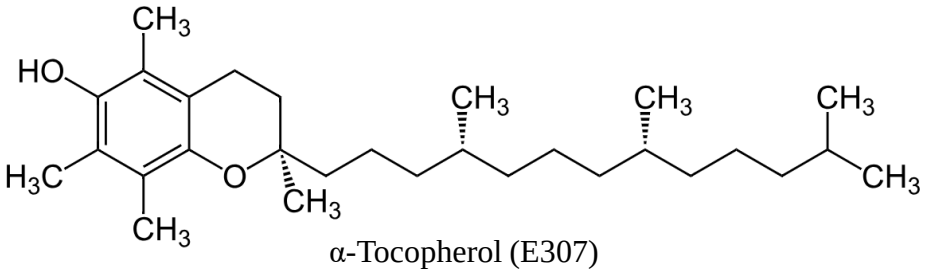

α-Tocopherol (E307)

Figure 1. Chemical structure of stearic acid and α-tocopherol

Cylindrically-shaped specimens were made from ferritic stainless steel (SS) type X4Cr13.

2.1. Pretreatment for working electrode

Ferritic stainless steel of type X4Cr13 with chemical composition expressed in % (wt.): C, 0.04, S, 0.02, Si, 0.471, Cr, 13.2, Ni, 0.307, Cu, 0.213). (C, 0.04, S, 0.02, Si, 0.471, Cr, 13.2, Ni, 0.307, Cu, 0.213) was used as a test material. The procedure for preparation of cylindrical samples, grinding, cleaning in an ultrasonic bath, repeated rinsing with distilled water and etching was the same as described in our previous study [46], as was the procedure for preparing the hydrophobic layer on the metallic surfaces, using a simple immersion technique [46]. The stainless steel samples (X4Cr13) were immersed in a 0.05 M ethanolic solution of SA (c = 0.05 mol L^{-1}) with and without the addition of various concentrations of α-Tocopherol (E307) at 0.5% (wt.), 1.0% (wt.) and 2.0% (wt.). This part of the experiment was carried out at room temperature. The corrosion resistance of the prepared hydrophobic coatings was tested within 3.0% (wt.) NaCl solution (to simulate sea water). The area of the electrode exposed to the electrolyte was 0.785 cm^2.

2.2. Electrochemical measurement

For electrochemical measurements, classical three electrode systems were used in a reference, counter and working electrode configuration (saturated calomel electrode (SCE), platinum electrode and ferritic steel samples). Potentiodynamic current-potential curves were recorded by automatically changing the electrode potential from -0.7 to the pitting potential (V/SCE) (when the protective hydrophobic layer was damaged) at a scanning-rate of 1 mVs^{-1}. To avoid ohmic drop, a Luggin capillary was used along with the reference electrode. EIS measurements were carried out within the 100 kHz–1 mHz frequency range at a steady open circuit potential (OCP) disturbed by an amplitude of 10 mV (more precisely, 10 points per decade and a 10 mV (peak to peak) amplitude of the excitation signal). Before each experiment, the stainless steel electrode was left at the open circuit potential in the corrosive solution for 60 mins in order to allow stabilization of the OCP. The measurements were performed at 25°C ± 1°C using a Solartron 1287 Electrochemical interface and a Gamry 600™ potentiostat/galvanostat controlled by an electrochemical program. Data were collected and analysed using CorrView, CorrWare, ZPlot and ZView software developed by Scribner Associates, Inc.

2.3. FTIR, SEM, (surface characterisation methods)

The morphologies of the self-assembled layers formed on the ferritic stainless steel surfaces were examined using a scanning electron microscope (SEM) (XL FEG/SFEG/SIRION). The wettability of stainless steel surfaces with and without self-assembled layers was measured with a commercial goniometer (Data Physics OCA 35, Germany). On the basis of ATR-FTIR analysis by Fourier transform infrared (SHIMADZU-IRAffinity-1), the presence of some functional groups in the prepared hydrophobic layer on the metal surface was confirmed. For comparison, the original solution (ethanolic solution of SA with the addition of 2.0% (wt.) of E307) was also analysed by ATR-FTIR.

3. RESULTS AND DISCUSSION

3.1. Electrochemical results

3.1.1 Electrochemical polarisation measurements

Potentiodynamic curves in a 3% (wt.) NaCl solution for bare stainless steel and a modified surface are shown in Fig.2. The modified SS surface showed a noticeable decrease in current density in the cathodic and anodic direction in comparison with the bare surface. In the anodic part of the polarization curves, a significant reduction in the anodic current density is observed, especially in the case when 1.0% (wt.) and 2.0% (wt.) of E307 was added to the ethanolic solution of stearic acid and also the shift of the broken pitting potential to the more noble potential. Moreover, the stability of the hydrophobic layer at these two particular concentrations of added E307 is observed; this is represented as a stable low current density within the relatively wide potential range in the anodic direction (Fig.2).

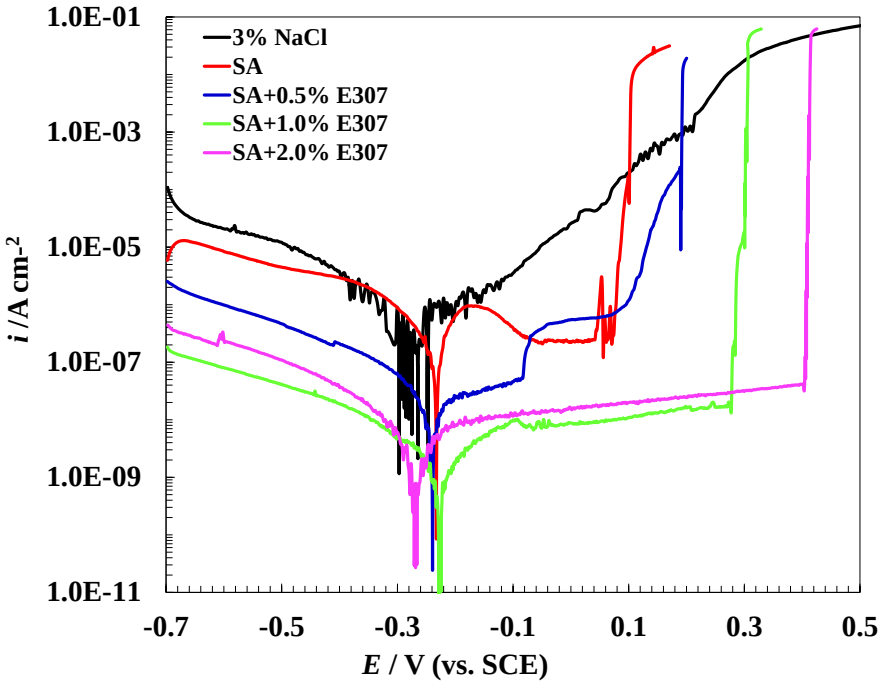

Figure 2. The influence of added E307 on the cathodic and anodic behaviour of SS type X4Cr13 for bare and modified surfaces in a solution of 3.0% (wt.) NaCl at 25ºC.

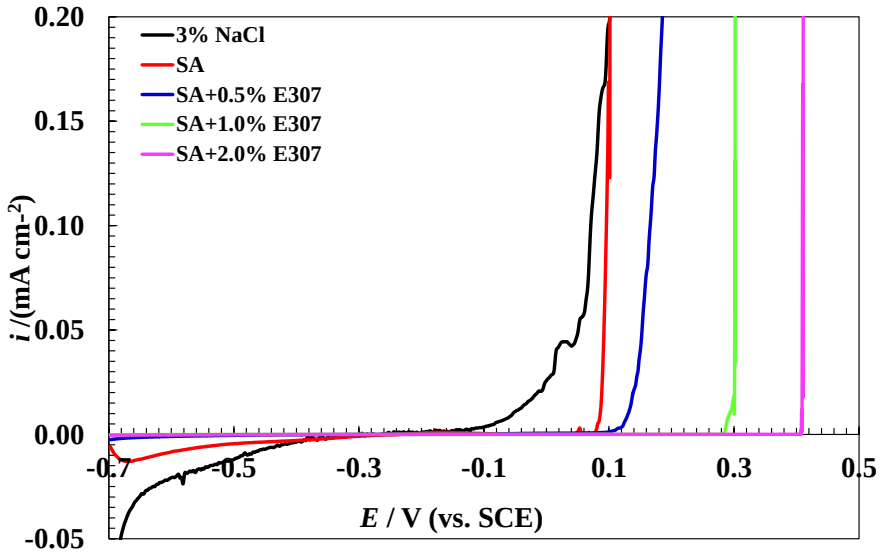

Figure 3. Potentiodynamic polarisation curves (1 mVs^{-1}) for SS type X4Cr13 for bare and modified surfaces in solution of 3.0% (wt.) NaCl at 25ºC.

The flat portion with constant current density are at approximately 550mV and 650mV, respectively (Fig.3). In other words, modified SS surfaces with the addition of E307 show higher pitting resistance compared to unmodified surfaces or those modified only in SA. Further, a three order of magnitude lower i_{corr} was observed for the chosen mixtures compared to the blank solution. A reduction in the cathodic current density was also observed, indicating that E307 in combination with stearic acid acts as a very effective mixed-type inhibitor. Finally, all the classical electrochemical

parameters, corrosion current density (i_{corr}), polarisation resistance (R_p) and corrosion potential (E_{corr}), together with values for inhibition efficiency (η_{icorr},η_{Rp},), obtained from these polarisation curves are collected in Table 1. All the parameters were determined with CorrView software.

Table 1. Kinetic parameters for corrosion of SS X4Cr13obtained from potentiodynamic polarisation curves for the bare and modified surfaces in the solution of 3.0 wt% NaCl at 25ºC.

Corrosive media 3% NaCl	i_{corr} **(nAcm^{-2})**	E_{corr} **(V vs. SCE)**	R_p **(MΩcm^2)**	$\eta_{i_{corr}}$	η_{R_p}
bare surface	**593.50**	**-0.270**	**0.022**	**-**	**-**
modified surface 0.05 M SA+x% (wt.) E307					
SA	**244.41**	**-0.233**	**0.065**	**58.82**	**66.28**
SA+0.5% (wt.)E307	**7.213**	**-0.238**	**1.136**	**98.77**	**98.01**
SA+1.0% (wt.)E307	**1.217**	**-0.223**	**12.441**	**99.71**	**99.82**
SA+2.0% (wt.)E307	**2.214**	**-0.272**	**6.573**	**99.63**	**99.66**

0[*]- 0.05 M SA

The inhibition efficiency η was calculated via the kinetic parameters measured during corrosion processes, as well as the polarisation resistance R_p, the corrosion current density i_{corr}, and the polarisation resistance $R_{p\text{-}EIS} = \Sigma R_i$; ($R_i = R_1, R_2, R_3$, from the EIS measurements) cf. Equations 1 and 2. Polarisation resistance η was calculated via Equation (2), where X = $R_{p,}$ $R_{p\text{-}EIS}$. Equation (1) was used in connection with the corrosion current density where Y = i_{corr} [46],

$$\eta\% = \left[1 - \frac{X'}{X}\right] \cdot 100 \quad (1)$$

$$\eta\% = \left[1 - \frac{Y}{Y'}\right] \cdot 100, \quad (2)$$

where the notations i_{corr} R_p and $R_{p\text{-}EIS}$ were used for measurements without inhibition action of the prepared hydrophobic layer, while the primed quantities i_{corr}*' Rp'* and $R_{p\text{-}EIS}$' were applied when measurements were performed on modified surfaces of SS type X4Cr13 in 3.0% (wt.) NaCl solution.

3.1.2. Electrochemical impedance measurements (EIS)

Electrochemical Impedance Spectroscopy is a non-destructive electrochemical technique that has become indispensable for the measurement of corrosion processes and the protective performance of various types of organic coatings and self-assembled layers. Impedance spectra can be divided into three different parts: the high frequency segment (HF) represents the properties of the coating; the second segment is approximately within the middle frequency region; and the low-frequency (LF) part

represents the reactions occurring at the bottom of the pores of the coating [47]. Figures 4 and 5 show Nyquist and Bode diagrams for SS type X4Cr13 in 3.0% (wt.) NaCl for treated and bare surfaces of SS. Bode plots represent impedance |*Z*| and phase changes (phase angle) of the frequency *f*, very often over a wide range of *f* values, on a logarithmic scale. For characterization of impedance measurements, two equivalent electrical circuits (EEC) were used representing two and three time constants respectively (Figs.6). Each time constant corresponds to the *R*–*CPE* element within the EEC models. Self-assembled layers have a random microstructure which is reflected in considerable heterogeneity on the surface. Thus, using a *CPE* element instead of a conventional capacitor is necessary, because this element includes the parameter *'n'*, with a value between 0.5-1. The values of the parameter *n*, which are approximately between 0.8-1, represent the non-homogeneous structure of the surface. When the value of *n* is close to 0.5, the diffusion characteristics of the process are more pronounced as a consequence of the porous paths within the surface layer, which allows the diffusion of the corrosive medium to the base matrix. *CPE*1 is a constant phase element representing the double layer capacitor; *CPE*2 is the capacitance of the prepared hydrophobic layer on the surface of SS type X4Cr13 substrate; and *CPE*3 is related to the diffusion capacitive component. The second element in the EEC models used to fit experimental EIS measurements is the resistance of individual elements within the EEC (R). In the EEC models, *R*s, R_1, R_2 and R_3 are electrolyte resistance, charge-transfer resistance, resistance of the hydrophobic layer and pore resistance, respectively. The models suggested have the least error and chi-square values (χ^2) between 0.001- 0.0035 or less. The value of R_s (150-200 Ωcm^2) includes any ohmic resistance between the electrode surface and the reference electrode. The impedance of the *CPE* is expressed as $\boldsymbol{Z_{CPE}} = \boldsymbol{Q}^{-1}(\boldsymbol{j\omega})^{-\boldsymbol{n}}$ [48]; the capacitances in μF cm^{-2} were calculated using the relationship $\boldsymbol{C_{dl}} = \left(\boldsymbol{Q}\cdot\boldsymbol{R}^{1-\boldsymbol{n}}\right)^{1/\boldsymbol{n}}$ [49]. The electrochemical parameters obtained from the EIS measurements are shown in Table 2.

The response at high frequencies (10^3 to 10^4 Hz) belongs to the first-time constant (R_1-CPE_1) and in general represents the charge-transfer process of SS dissolution, with elements showing the impedance of the interface reaction between the film and substrate.

Table 2. Impedance parameters and corresponding inhibition efficiencies for the corrosion of SS type X4Cr13 in 3.0 wt% NaCl at 25ºC for the bare and modified surfaces.

Corrosive media 3% (wt.)NaCl	R_1 (kΩ cm^2)	n_1	C_1 (μFcm^{-2})	R_2 (MΩ cm^2)	n_2	C_2 (μFcm^{-2})	R_3 (MΩ cm^2)	n_3	C_3 (μFcm^{-2})	$R_{p\text{-}EIS}$ (MΩ cm^2	% $\eta_{Rp\text{-}EIS}$
blank	**380.07**	**0.824**	**35.35**	**0.018**	**0.482**	**3297.910**	/	/	/	**0.398**	
SA	**16.68**	**0.939**	**0.045**	**1.736**	**0.615**	**1.688**	**0.644**	**0.517**	**0.5504**	**2.40**	**83.42**
SA+0.5%E307	**110.06**	**0.922**	**0.039**	**11.002**	**0.829**	**0.431**	**0.909**	**0.588**	**1.181**	**12.03**	**96.69**
SA+1.0%E307	**128.06**	**0.870**	**0.041**	**22.380**	**0.904**	**0.306**	/	/	/	**22.51**	**98.23**
SA+2.0%E307	**120.90**	**0.906**	**0.029**	**26.790**	**0.989**	**0.180**	/	/	/	**26.91**	**98.52**

The anti-corrosion performance of a coating depends on its ability to prevent electrolyte permeation into the coating/metal interface. Coatings with excellent barrier properties maintain highly capacitive behaviour through many years of exposure to weather. Furthermore, |*Z*| is at least 10^9 Ohms (Ω) at the lowest frequency, 10^{-3} Hz. Graphically, this is a line with a slope of -1 for |*Z*| and a value of

the phase angle very close to -90° at all frequencies. Deviations from this in the low frequency region indicate resistive behaviour. For perfect resistor behaviour, the value of the phase angle should be equal to 0°. It has been shown that with broadening area where predominates capacitor behaviour and simultaneous reduction of the resistance zone shows on the successfully hindering against to the penetration of electrolytes and corrosive agents to the surface.

In contrast, increased resistive behaviour is indicative of coating degradation, with possible delimitation in the interior of the protective coating/layer, which has a continuation as a corrosion reaction of the underlying steel substrate. The second segment is at medium frequencies (10 Hz) where a linear relationship between log |Z| vs. log *f* with a slope varying from 0.62-0.99 and with a phase angle between -82º and -85º (not far from -90º) was observed (Fig.5a). SS type X4Cr13, coated with a prepared hydrophobic layer, with the addition of 1% (wt.) or 2% (wt.) of E307, has the largest capacitor zone (Figs.5), which leads to better blocking properties of the coating than when E307 is not added to the ethanolic solution of stearic acid or at the lowest added concentration of 0.5% (wt.). With increasing concentrations of E307, the R_2 values increased and the capacitance CPE_2 of the prepared hydrophobic layer decreased noticeably compared to when just SA was used for modification of the SS surface (Table 2).

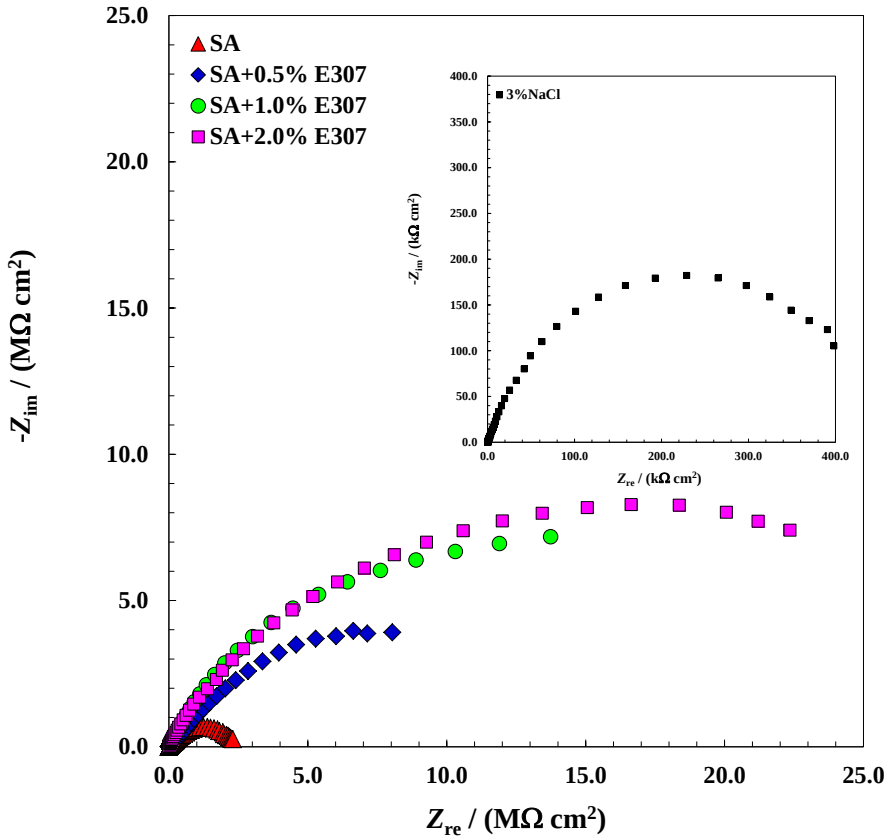

Figure 4. EIS Nyquist plots for SS type X4Cr13 for bare and modified surface in solution of 3.0 wt% NaCl at 25ºC. (The modified surfaces were prepared by immersion of SS type X4Cr13 in 0.05 M stearic acid in ethanol with and without addition of E307).

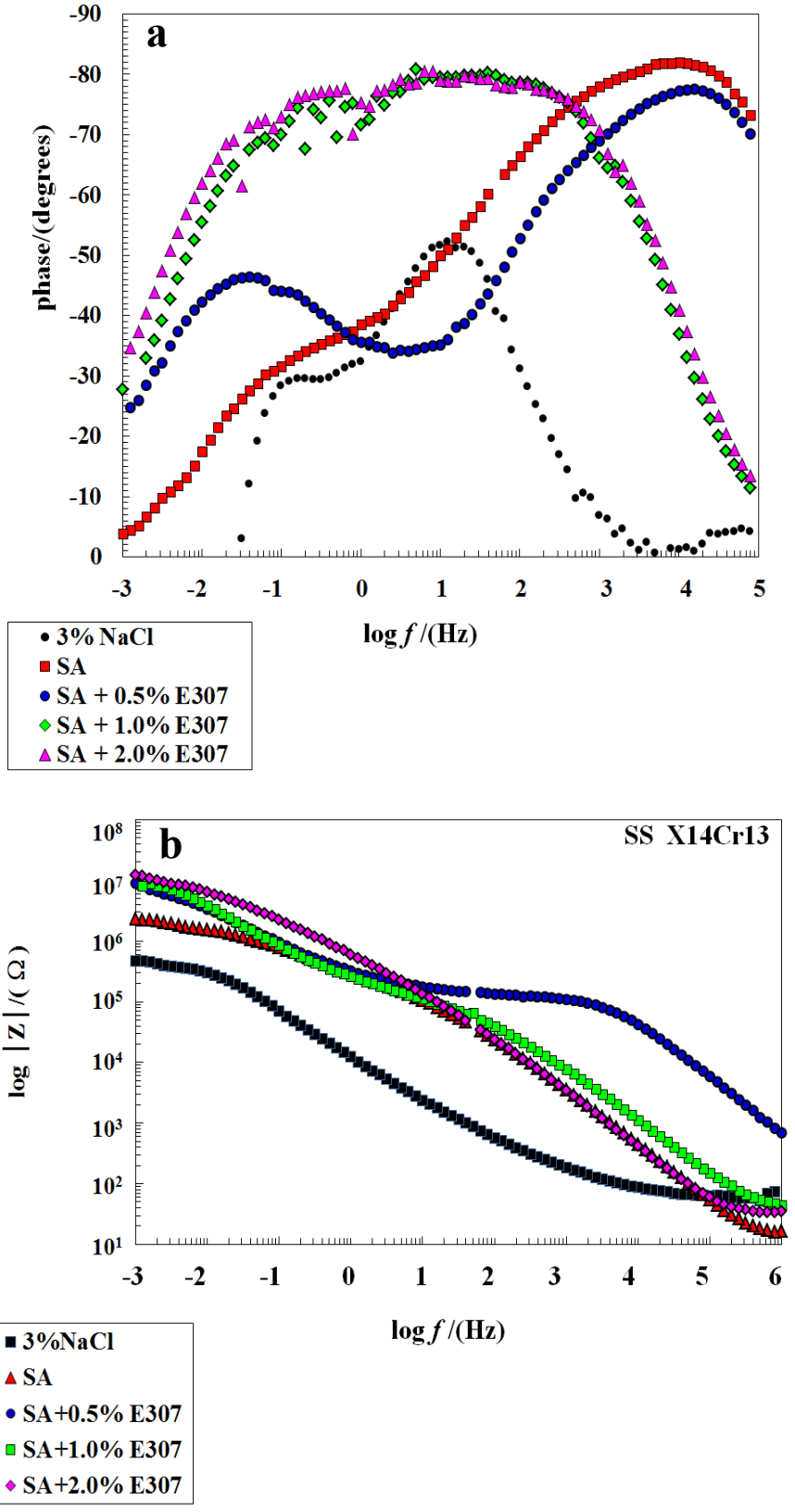

Figure 5. Bode plots and the electrochemical equivalent circuit used for simulating the impedance data for for SS type X4Cr13 for bare and modified surface in solution of 3.0 wt% NaCl at 25ºC.

The notation R_3-CPE_3 represents the third time constant, (within the low frequency region) and is ascribed to the diffusion process; the parameter n_3 was found to be around 0.5. This was observed at the lowest concentration of E307 in the ethanolic solution of SA. The hydrophobic layer formed under these conditions is more porous and therefore more vulnerable to corrosion processes. Due to all these factors, and because the |Z| value in the low-frequency region (and consequently the $R_{p\text{-}EIS}$) increases when E307 is added, we speculate that the metal ions (mostly Fe and Cr), have diffused through the pores of the prepared hydrophobic layer, reacted with the oxygen to form oxide, and filled the gaps within the hydrophobic layer. This could be confirmed by increasing the values of the impedance parameters R_2 and R_3. The best protective effect for the prepared hydrophobic layer was achieved when the concentration of added E307 was 2.0% (wt.) (Table 2).

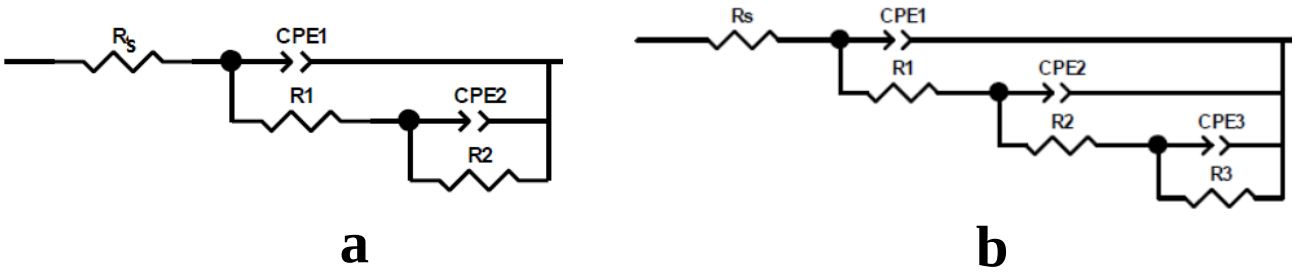

Figure 6. Equivalent circuits used in EIS data analyses.

Fig.6a – Equivalent circuit used in the analysis of EIS data of SS type X4Cr13 in blank solution (3.0% (wt.) NaCl) and when modified surfaces were prepared by immersion of SS in 0.05 M SA acid in ethanol with addition of 1.0% (wt.) and 2% (wt.) of E307.

Fig.6b – Equivalent circuit used in the analysis of EIS data for modified surface of SS prepared by immersing the sample in an ethanolic solution of SA without and with addition of 0.5% (wt.) of E307.

3.2. Wettability of a high-level hydrophobic surface

The surface microstructures of bare and hydrophobic samples of SS type X4Cr13, as observed by SEM, is demonstrated in Figure 7. The images of the water droplets on the modified surfaces, given within rectangles, indicate the hydrophobicities of the modified surfaces, with values of CA very close to those of super-hydrophobic surfaces (CA ≥150°). The obtained values for contact angle are also very similar to those in our previous study on copper [46], confirming that the prepared hydrophobic layers on the SS could have similar physical characteristics to those of copper. The visual appearance of the flower-like clusters is completely different than those obtained for the copper surface (much more expressive and look like as a real blossom). Hao [50] reported that such regularly ordered flower-like structures can trap a large amount of air, which is expected for this high level of surface hydrophobicity.

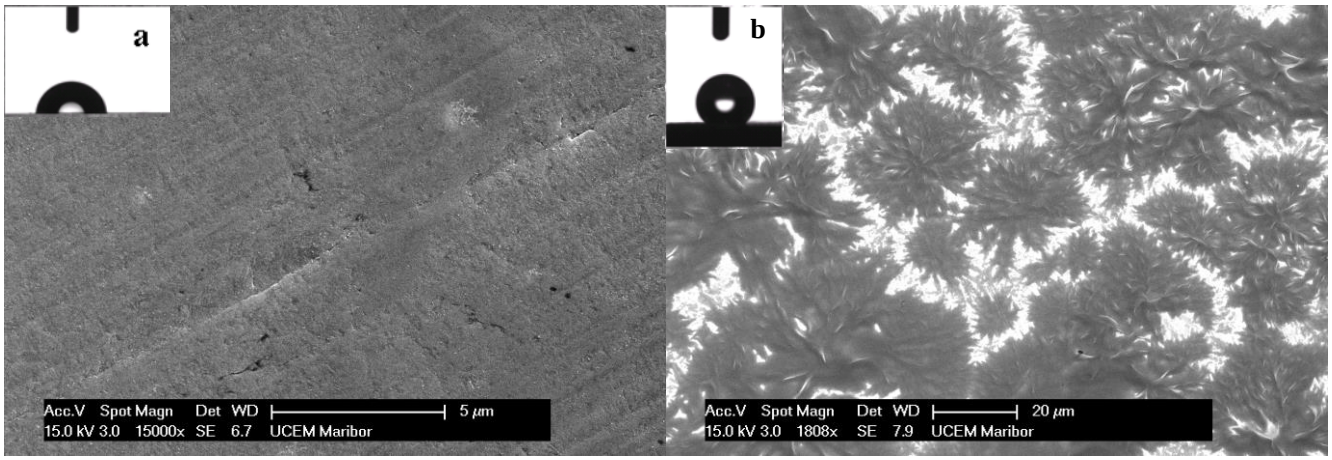

Figure 7. SEM of the untreated and modified surface of SS type X4Cr13 (a) untreated and etched surface (CA=71.5°±3), (b) modified surface in SA solution with the addition of 2% of Vitamin E for one hour (CA=138.7°±3).

3.3. ATR–FTIR analysis

The goal of the ATR-FTIR analysis was to prove the presence of a-tocopherol (E307) in modified hydrophobic films on SS type X4Cr14 surfaces, because inhibition efficiency noticeable increased with addition of E307. The FTIR reflectance spectrum of prepared hydrophobic layers on SS surface type X4Cr13 after immersion in an ethanolic solution of SA with of E307 is shown in Figs. 8. As Y.B. Che Man [51] reported, the α-tocopherol spectrum exhibited an absorption band at the wavelength 3473 cm^{-1} for OH stretching bands [52], 2868 cm^{-1} for asymmetric and symmetric stretching vibrations of the CH_2 and CH_3 [53], and as reported by Solano Valderrama [54], 1461 cm^{-1} indicates phenyl skeletal and methyl asymmetric bending (1460 cm^{-1}), 1378 cm^{-1} for methyl symmetric bending, 1262 cm^{-1} for $–CH_2$, 1086 cm^{-1} for plane bending of phenyl and 919 cm^{-1} for *trans* $=CH_2$ stretching [54].

On the basis of all wavelengths which is characteristic for E307 (mentioned above) and the absorption bands in the Fig.8a we can confirm the presence of E307 in the hydrophobic layers on SS surface type X4Cr13. The band which appeared at 1710 $cm^{-}1$ is attributed to C=O stretching [55]. Esterification of stearic acid and E307 could be the main reason for the appearance of that strong band which can be seen in the Fig.8a.

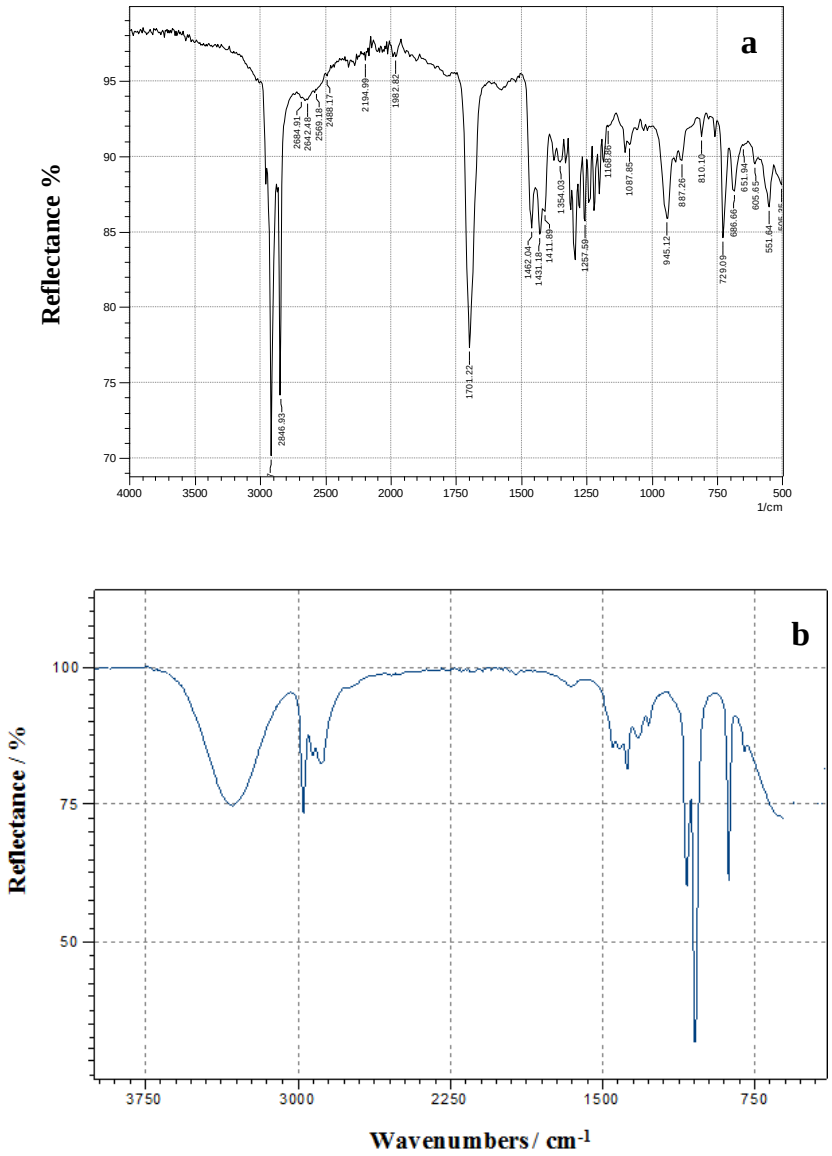

Figure 8. ATR-FTIR spectra (a) modified surface of SS type X4Cr13 in ethanolic solution of SA with the addition of 2.0 wt % of E307 for one hour, (b) for ethanolic solution of SA + 2.0 wt% of E307.

4. CONCLUSION

Modification of a stainless-steel (SS) X4Cr13 surface was achieved by immersion in ethanol solutions of stearic acid with and without the addition of α-tocopherol. We observed a double effect: a hydrophobic and corrosion-resistant surface of SS type X4Cr13 in a solution of 3.0% (wt.) NaCl at 25ºC.

The water contact angle (CA) for the modified layers formed on the surface of SS type X4Cr13 in the presence of stearic acid alone and in combination with E307 was significantly larger than that for the bare surface of SS. The significant increase in contact angle indicates that the morphology

effectively repelled water (in our case water solution of 3.0% (wt.) NaCl), which was confirmed with potentiodynamic and EIS measurements.

Potentiodynamic polarisation measurements show that the inhibition effectiveness of X4Cr13 reached ≈ 68% when surfaces were modified in stearic acid alone (EIS measurements ≈ 82%), while the values with addition of E307 increased to more than 99.0% for both methods. We speculate that the film formed almost completely stops the destructive function of corrosion reactions until degradation of the film begins.

ACKNOWLEDGEMENTS
This work was financially supported by Slovenian Research Agency under research project "Physico-Chemical Processes on the Surface Layers and Application of Nanoparticles" (P2-0006).

References

1 J. García, H.R. Fischer, S. Van der Zwaag, *Progress in Organic* Coatings, 72 (2011) 211.
2 S. Thomas, N. Birbilis, M.S. Venkatraman, I.S. Cole, *Corrosion Science*, 69 (2013) 11.
3 H. Hornberger, S. Virtanen, A.R. Boccaccini, *Acta Biomaterialia*, 8 (2012) 2442.
4 M.J. O'Keefe, W.G. Fahrenholtz, B.S. Curatolo, *Metal Finishing*, 108 (2010) 28.
5 M. Ali, M.A. Hussein, N. Al-Aqeeli, *Journal of Alloys and Compounds,* 792 (2019) 1162.
6 H. Wall, L. Wadsö, *Marine Structures*, 33 (2013) 21.
7 M. Talha, Y. Ma, P. Kumar, Y. Lin, A. Singh, *Colloids and Surfaces B: Biointerfaces*, 176 (2019) 495.
8 T. He, Y. Wang, Y. Zhang, Q. Iv, T. Xu, T. Liu, *Corrosion Science*, 51 (2009) 1757.
9 M. Qu, B. Zhang, S. Song, L. Chen, J. Zhang, X. Cao, *Advanced Functional Materials,* 17 (2009) 593.
10 T. Liu, S. Chen, S. Cheng, J. Tian, X. Chang, Y. Yin, *Electrochim Acta*, 52 (2007) 8003.
11 R. Fuchs-Godec, *Electrochim Acta*, 52 **(**2007) 4974.
12 R. Fuchs-Godec, *Electrochim Acta*, 54 (2009) 2171.
13 R. Fuchs-Godec, *Industrial & Engineering Chemistry Research*, 49 (2010) 6407.
14 R. Fuchs-Godec, M.G. Pavlović, *Corrosion Science*, 58 (2012) 192.
15 A.Y. El-Etre, M. Abdallah, *Corrosion Science*, 42 (2000) 731.
16 A. Rodríguez-Torres, O. Olivares-Xometl, M. G. Valladares-Cisneros, J. G. González-Rodríguez, *International Journal of Electrochemical Science*, 13 (2018) 3023.
17 A. Pasupathy, S. Nirmala, G. Abirami, A. Satish, R. P. Milton, *International Journal of Scientific and Research Publications*, 4 (2014) 1.
18 Xi. Jiang, C. Lai, Z. Xiang, Ya. Yang, B. Tan, Z. Long, L. Liu, Y. Gu, W. Yang, X. Chen, *International Journal of Electrochemical Science*, 13 (2018) 3224.
19 S. Martinez, I. Stern, *Journal of Applied Electrochemistry*, 31 (2001) 973.
20 G. Khan, K.M.S. Newaz, W. J. Basirun, H.B.M. Ali, F.L. Faraj, G.M. Khan, *Journal of Applied Electrochemistry*,10 (2015) 6120.
21 E. Khamis, N. Al-Andis, *Materialwissenschaft und Werkstofftechnik*, 33 (2002) 550.
22 A.M. Alsabagh, M.A. Migahed, M. Abdelraouf, E.A. Khamis, *International Journal of Electrochemical Science*, 10 (2015) 1855.
23 M. Kliskic, J. Radosevic, S. Gudic, V. Katalinic, *Journal of Applied Electrochemistry*, 30 (2000) 823.
24 R. Fuchs–Godec, M.G. Pavlović, M.V. Tomić, *International Journal of Electrochemical Science*, 10 (2015) 10502.

25 R. Fuchs–Godec, M.G. Pavlović, M.V. Tomić, *International Journal of Electrochemical Science*, 8 (2013) 1511.
26 M.B. Petrović Mihajlović, M.M. Antonijević, *International Journal of Electrochemical Science*, 10 (2015) 1027.
27 C. Verma, J. Haque, M. A. Quraishi, E. E. Ebenso, *Journal of Molecular Liquids*, 275 (2019) 18.
28 A. Aloysius, R. Ramanathan, A. Christy, S. Baskaran, N. Antony, *Egyptian Journal of Petroleum*, 27 (2018) 371.
29 A.R. Hoseinzadeh, I. Danaee, M.H. Maddahy, *Zeitschrift für Physikalische Chemie*, 227 (2013) 403.
30 R. Solmaz, *Corrosion Science*, 81 (2014) 75.
31 K. Qiao,Y. Wu, X. Liu, *Advanced Materials Research*, 463–464 (2012) 895.
32 Z. Shi, Y. Ouyang, R. Qiu, S. Hu, P. Wang, *Progress in Organic Coatings*, 131 (2019) 49.
33 S. Wang, L. Feng, L. Jiang, *Advanced Materials*, 18 (2006) 767.
34 Z. Yang, X. Liu, Y. Tian, *Colloids and Surfaces A: Physicochemical and Engineering Aspects*, 560 (2019) 205.
35 A.M.A. Mohamed, A.M. Abdullah, N.A. Younan, *Arabian Journal of Chemistry*, 8 (2015) 749.
36 S. Niu, Y. Fang, R. Qiu, Z. Qiu, Y. Xiao, P.Wang, M. Chen, *Colloids and Surfaces A: Physicochemical and Engineering Aspects*, 550 (2018) 65.
37 T. He, Y. Wang, Y. Zhang, Q. Iv, T. Xu, T. Liu, *Corrosion Science*, 51 (2009) 1757.
38 L. Li, V. Breedveld, D.W. Hess, *ACS Applied Materials & Interfaces*, 4 (2012) 4549.
39 W.F. Ng, M.H. Wong, F.T. Cheng, *Surface & Coatings Technology*, 204 (2010) 1823.
40 L.B. Boinovich, S.V. Gnedenkov, D.A. Alpysbaeva, V.S. Egorkin, A.M. Emelyanenko, S.L. Sinebryukhov, A.K. Zaretskaya, *Corrosion Science*, 55 (2012) 238.
41 Z. Cao, F. Lu, P. Qiu, F. Yang, H. Zhong, *Colloids and Surfaces A: Physicochemical and Engineering Aspects*, 555 (2018) 372.
42 A. Dehghani, G. Bahlakeh, B. Ramezanzadeh, M. Ramezanzadeh, *Journal of Molecular Liquids*, 279 (2019) 603.
43 G. Kılınççeker, S. Çelik, *Ionics*, 19 (2013) 1655.
44 L.J. Chen, M. Chen, H.D. Zhou, J.M. Chen, *Applied Surface Science*, 255 (2008) 3459.
45 J. Qu, C. Yu, R. Cui, J. Qin, Z. Cao, *Surface and Coatings Technology*, 354 (2018) 236.
46 R. Fuchs-Godec, G. Zerjav, *Corrosion Science*, 97 (2015) 16.
47 H. R. Tiyyagura, R. Fuchs-Godec, S. Gorgieva, S. Arthanari, M. K. Mohan,V. Kokol, *Journal of Materials Research*, 33 (2018) 1449.
48 A. Popova, M. Christov, *Corrosion Science*, 48 (2006) 3208.
49 S. Martinez, M. Metikos-Hukovic, *Journal of Applied Electrochemistry*, 33 (203) 1137.
50 L. Hao, Y. Sirong, H. Xiangxiang, *Chemical Engineering Journal*, 283 (2016) 1443.
51 Y.B. Che Man, W. Ammawath, M.E.S. Mirghani, *Food Chemistry*, 90 (2005) 323.
52 Y.B. Che Man, M.E.S. Mirghani, *Journal of the American Oil Chemists' Society*, 77 (2000) 631.
53 M.D. Guillen, N. Cabo, Journal of the Science of Food and Agriculture, 75 (1997) 1.
54 A.C. Solano Valderrama, G.C. Rojas De, *American Journal of Analytical Chemistry*, 8 (2017) 726.
55 S. Li, X. Zhang, Y. Shan, D. Su, Q. Ma, R. Wen, J. Li, *Food Chemistry*, 218 (2017) 231.